DALTON
FULL PAPER

Copper(II) complexes of 2,6-bis(3-*tert*-butylpyrazol-1-yl)pyridine

Nayan K. Solanki,[a] Eric J. L. McInnes,[b] David Collison,[b] Colin A. Kilner,[c] John E. Davies[a] and Malcolm A. Halcrow*[c]

[a] *Department of Chemistry, University of Cambridge, Lensfield Road, Cambridge, UK CB2 1EW*
[b] *CW EPR Service Centre, Department of Chemistry, University of Manchester, Oxford Road, Manchester, UK M13 9PL*
[c] *School of Chemistry, University of Leeds, Woodhouse Lane, Leeds, UK LS2 9JT. E-mail: M.A.Halcrow@chem.leeds.ac.uk*

Received 7th December 2001, Accepted 13th February 2002
First published as an Advance Article on the web 26th March 2002

The stereochemical preferences of copper complexes of 2,6-bis(3-*tert*-butylpyrazolyl)pyridine (L^1Bu^t) have been investigated. The single crystal X-ray structures of $[\{Cu(\mu\text{-}Cl)(L^1Bu^t)\}_2][BF_4]_2$ (**3a**), $[\{Cu(\mu\text{-}Cl)(OH_2)(L^1Bu^t)\}_2][BF_4]_2$ (**3b**) and $[Cu(NCMe)_2(L^1Bu^t)][BF_4]_2$ (**4**) show distorted tetragonal geometries at Cu, with one or two axial solvent and/or BF_4^- ligands. The Cu centres in **3a** and **3b** are weakly associated into dimers, through axial Cu–Cl ··· Cu bridging. Single crystals of **4** undergo an unusual substitution of their MeCN ligands upon exposure to air, yielding $[Cu(OH_2)_2(L^1Bu^t)][BF_4]_2$ (**1**). A combination of UV/vis, EPR and conductivity studies has shown that Cu(II)-bound L^1Bu^t is labile in solution. Susceptibility data show that the Cu ions in **3a** are weakly antiferromagnetically coupled through the Cl^- bridges, although this compound exhibits a spin-triplet EPR spectrum in the solid. Cyclic voltammograms of **3a** and **4** in MeCN–0.1 M $NBu^n_4BF_4$ confirm the lability of Cu-bound L^1Bu^t.

Introduction

We have recently reported that the complex $[Cu(L^1Mes)_2][ClO_4]_2$ exhibits an unusual $\{d_{z^2}\}^1$ ground state in the solid and solution phases, corresponding to an axially compressed molecular structure.[1–3] This is the first molecular six-coordinate Cu(II) complex that has been rigorously shown to possess this property,[4] although we have subsequently shown that it can also be induced using other, related ligand systems.[5] The $\{d_z^2\}^1$ ground state probably reflects steric repulsion between the mesityl groups of one coordinated ligand, and the pyridine ring of the other. Supporting this idea, the unsubstituted complex $[Cu(L^1H)_2][BF_4]_2$ adopts the more usual pseudo-Jahn–Teller elongated $\{d_{x^2-y^2}\}^1$ electronic structure.[1,6,7]

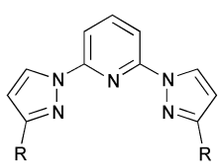

L^1R

In the light of the above results, we were interested in examining the effects of larger distal substituents on the copper chemistry of L^1R. We now describe the syntheses and structural, spectroscopic and (in one case) magnetochemical characterisation of some Cu(II) complexes of L^1Bu^t.[8] One of these compounds undergoes an unusual solid state ligand substitution reaction upon exposure to air, while another exhibits an interesting case of crystallographic polymorphism.

Results and discussion

Syntheses and crystal structures

Treatment of $Cu[BF_4]_2{\cdot}6H_2O$ with 1–3 equivalents of L^1Bu^t in MeCN yields, in all cases, a purple solution from which a mauve microcrystalline solid can be isolated by precipitation with Et_2O. This solid analyses as $[Cu(OH_2)_2(L^1Bu^t)][BF_4]_2$ (**1**) after drying. This implies that the ligand *tert*-butyl groups are too bulky to permit coordination of a second equivalent of L^1Bu^t to copper. In an alternative approach, $CuCl_2$ was reacted with 1–3 molar equivalents of L^1Bu^t in refluxing MeOH, which only afforded the insoluble yellow solid $[CuCl_2(L^1Bu^t)]$ (**2**) contaminated with unreacted L^1Bu^t. Compound **2** was more conveniently prepared by reaction of anhydrous $CuCl_2$ with 1 molar equivalent of L^1Bu^t in refluxing MeCN. Treatment of **2** with 2 molar equivalents of $AgBF_4$ in the presence of L^1Bu^t in MeCN or $MeNO_2$ yielded **1** as the only isolable product.

Treatment of **2** with an equimolar amount of $AgBF_4$ in MeCN at room temperature gave a brown solution. Following filtration and concentration of this solution, vapour diffusion of Et_2O yielded a mixture of large green and smaller amber crystals, both with a cubic morphology, with the green product being *ca.* 3 times as abundant as the amber one. Microanalysis and X-ray crystallography (see below) formulated these compounds as $[\{Cu(\mu\text{-}Cl)(L^1Bu^t)\}_2][BF_4]_2$ (**3a**, green) and $[\{Cu(\mu\text{-}Cl)(OH_2)(L^1Bu^t)\}_2][BF_4]_2$ (**3b**, amber). Since only **3a** formed crystals that were large enough to be separated manually from the product mixture in any quantity, all spectroscopic and magnetic measurements were carried out using this compound.

Both **3a** and **3b** crystallise in $P2_1/c$, and exhibit similar unit cell dimensions (see Experimental section). Each structure contains $[CuCl(L^1Bu^t)]^+$ centres with three basal imine donors and a basal chloro ligand, that are weakly associated into dimers through long-range axial Cu ··· Cl interactions across a crystallographic inversion centre. In **3a** the sixth Cu coordination site is occupied by the disordered BF_4^- anion, with Cu–F distances of 2.40–2.45 Å (Fig. 1, Table 1). In **3b**, however, the sixth ligand is a water molecule, with Cu(1)–O(27) = 2.269(3) Å (Fig. 2). Each H atom of this aqua ligand is hydrogen-bonded to one (disordered) F atom of a different BF_4^- anion (not shown in Fig. 2), leading to a 1-D hydrogen-bonded polymeric lattice structure.

Table 1 Selected bond lengths (Å) and angles (°) for [{Cu(μ-Cl)-(L^1Bu^t)}$_2$][BF_4]$_2$ (**3a**) and [{Cu(μ-Cl)(OH_2)(L^1Bu^t)}$_2$][BF_4]$_2$ (**3b**). Primed atoms are related to unprimed atoms by the relation $1 - x$, $1 - y$, $1 - z$

	3a[a] [X = F(28A), F(28B)]	**3b** [X = O(27)]
Cu(1)–N(2)	1.9425(18)	1.961(3)
Cu(1)–N(9)	2.1134(18)	2.120(3)
Cu(1)–N(18)	2.1011(17)	2.127(3)
Cu(1)–Cl(26)	2.1978(5)	2.199(3)
Cu(1)–X	2.400(9), 2.453(10)	2.269(3)
Cu(1)–Cl(26′)	3.0465(6)	3.523(2)
Cu(1) ··· Cu(1′)	4.0069(5)	4.500(6)
N(2)–Cu(1)–N(9)	78.59(7)	78.31(11)
N(2)–Cu(1)–N(18)	78.90(7)	78.57(12)
N(2)–Cu(1)–Cl(26)	157.46(6)	149.02(8)
N(2)–Cu(1)–X	96.50(16), 85.5(2)	94.57(13)
N(2)–Cu(1)–Cl(26′)	75.96(5)	71.82(10)
N(9)–Cu(1)–N(18)	154.42(7)	155.81(10)
N(9)–Cu(1)–Cl(26)	102.40(5)	101.45(9)
N(9)–Cu(1)–X	85.9(2), 80.8(3)	86.49(11)
N(9)–Cu(1)–Cl(26′)	98.29(5)	106.76(8)
N(18)–Cu(1)–Cl(26)	103.05(5)	102.00(10)
N(18)–Cu(1)–X	84.8(3), 85.5(3)	88.36(12)
N(18)–Cu(1)–Cl(26′)	87.84(5)	72.32(9)
Cl(26)–Cu(1)–X	106.03(15), 117.0(2)	116.40(11)
Cl(26)–Cu(1)–Cl(26′)	81.652(18)	78.81(9)
X–Cu(1)–Cl(26′)	170.4(2), 161.2(2)	158.03(7)
Cu(1)–Cl(26)–Cu(1′)	98.348(15)	101.19(9)

[a] The apical BF_4^- ligand is disordered over two equally occupied orientations. The two values quoted for bonds and angles to this ligand correspond respectively to the two disorder orientations of the donor F atom, F(28A) and F(28B).

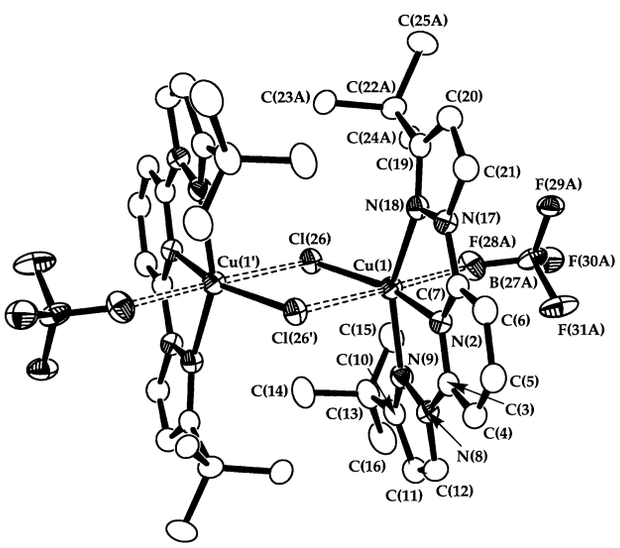

Fig. 1 View of the weakly associated [{Cu(μ-Cl)(L^1Bu^t)}$_2$][BF_4]$_2$ dimer in the structure of **3a**, showing the atom numbering scheme employed. Only one orientation of the disordered *tert*-butyl group and BF_4^- anion are shown. Thermal ellipsoids are drawn at the 50% probability level. For clarity, all C-bound H atoms have been omitted. Primed atoms are related to unprimed atoms by the relation $1 - x$, $1 - y$, $1 - z$.

The [CuCl(L^1Bu^t)]$^+$ moieties in **3a** and **3b** have similar geometries. The Cu(1)–Cl(26) bond lengths are indistinguishable in the two structures, although the distances Cu(1)–N(2) and Cu(1)–N(18) are slightly longer in **3b** than in **3a** (Table 1); the reason for this is unclear. The Cl^- ligand in both structures lies proud of the plane formed by the three L^1Bu^t N-donors, which is exemplified by the N(2)–Cu(1)–Cl(26) angles of 157.46(6)° for **3a**, and 149.02(8)° for **3b**, compared to 180° for a regular tetragonal geometry. The bridging Cu ··· Cl′ contacts (symmetry relation $1 - x$, $1 - y$, $1 - z$) are 3.0465(6) Å for **3a** and 3.523(2) Å for **3b**. The difference between these two values might reflect the increased *trans*-influence of the aqua ligand in **3b** compared to a BF_4^- ion in **3a**.

Table 2 Selected bond lengths (Å) and angles (°) for [Cu($NCMe)_2$-(L^1Bu^t)][BF_4]$_2$ (**4**). F(41A) and F(41B) are two different disordered sites for the same F atom

Cu(1)–N(2)	1.933(4)
Cu(1)–N(9)	2.103(4)
Cu(1)–N(18)	2.151(4)
Cu(1)–N(26)	1.947(4)
Cu(1)–N(29)	2.184(4)
Cu(1)–[F(41A), F(41B)]	2.669(4), 2.66(2)
N(2)–Cu(1)–N(9)	79.10(16)
N(2)–Cu(1)–N(18)	78.27(16)
N(2)–Cu(1)–N(26)	153.26(16)
N(2)–Cu(1)–N(29)	107.25(15)
N(2)–Cu(1)–[F(41A), F(41B)]	78.36(16), 69.7(4)
N(9)–Cu(1)–N(18)	157.33(15)
N(9)–Cu(1)–N(26)	98.16(16)
N(9)–Cu(1)–N(29)	98.09(15)
N(9)–Cu(1)–[F(41A), F(41B)]	96.26(17), 80.8(4)
N(18)–Cu(1)–N(26)	101.47(16)
N(18)–Cu(1)–N(29)	89.80(14)
N(18)–Cu(1)–[F(41A), F(41B)]	77.96(15), 90.2(4)
N(26)–Cu(1)–N(29)	99.48(16)
N(26)–Cu(1)–[F(41A), F(41B)]	75.70(16), 83.5(4)
N(29)–Cu(1)–[F(41A), F(41B)]	165.35(17), 176.9(4)

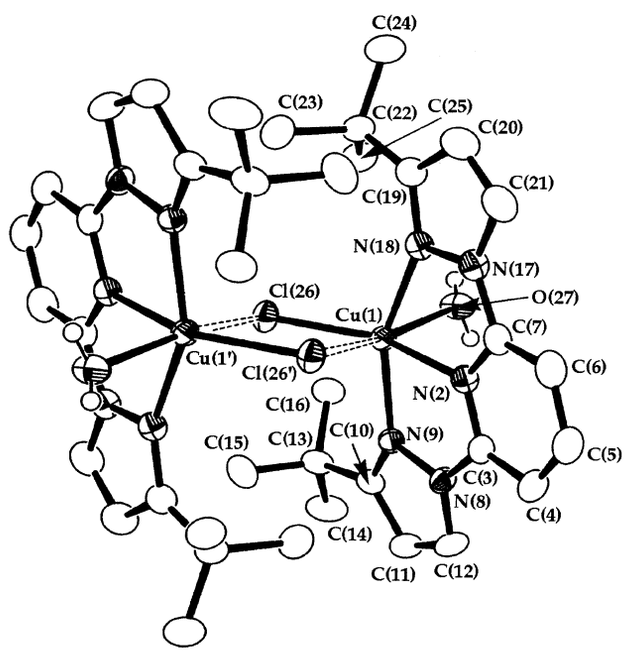

Fig. 2 View of the weakly associated [{Cu(μ-Cl)(OH_2)(L^1Bu^t)}$_2$]$^{2+}$ dimer in the structure of **3b**, showing the atom numbering scheme employed. Details as for Fig. 1. Primed atoms are related to unprimed atoms by the relation $1 - x$, $1 - y$, $1 - z$.

The molecular structure of **4** also shows a distorted tetragonal Cu(II) centre, with three basal imine N donors from the tridentate ligand and one basal MeCN ligand (Table 2, Fig. 3). The two axial positions are occupied by a second MeCN ligand at a relatively short Cu–N distance of 2.184(4) Å, and by longer contacts of 2.669(4) and 2.66(2) Å to one F atom which is disordered over two sites. The bond angles at copper are approximately that required for an octahedral geometry, with distortions for the L^1Bu^t bite angle, which averages to 78.7(2)°, and the disordered anion.

Exposure of crystals of **4** to air results in rapid loss of crystallinity, affording after a few hours a compound analysing as [Cu($OH_2)_2$(L^1Bu^t)][BF_4]$_2$, which is spectroscopically identical to **1**. The complete loss of MeCN from the solid was confirmed by microanalysis and by IR spectroscopy, which showed no bands

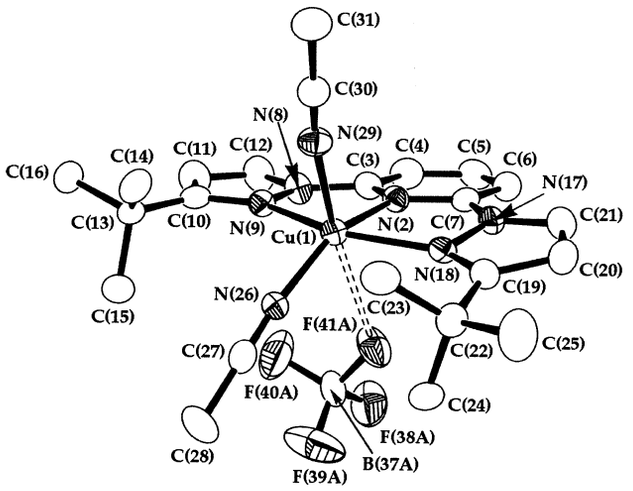

Fig. 3 View of the $[Cu(NCMe)_2(L^1Bu^t)(BF_4)]^+$ moiety in the structure of **4**, showing the atom numbering scheme employed. Only the major orientation of the disordered BF_4^- anion is shown. Details as for Fig. 1.

assignable to coordinated or lattice MeCN. The packing diagram of crystalline **4** shows no channels within the lattice that would allow ready access of water to the copper centres, or permit facile loss of MeCN from the bulk material. Presumably, therefore, this unusual reaction is triggered by loss of crystallinity following an initial substitution of MeCN ligands at the crystal surface. Its instability to MeCN loss has unfortunately prevented any other characterisation of **4** as a pure solid.

Conductivity measurements and UV/vis spectroscopy

Solution UV/vis and conductivity data for the Cu(II) compounds in this study, in both MeCN and $MeNO_2$ solutions, are listed in the Experimental section. Conductivity measurements for **1**–**3a** were consistent with their being a 1 : 2 electrolyte (**1**), a non-electrolyte (**2**) and a 1 : 1-electrolyte (**3a**, *i.e.* one anion per Cu(II) centre) in both solvents.[9] These measurements are consistent with the solid state molecular structures of **3a**, **3b** and **4**, and demonstrate that solvolysis of the Cl^- ligands does not occur upon dissolution of **2** or **3a**.

In the light of the conductivity data, it is interesting that **1**–**3a** are all strongly solvatochromic. While all three complexes show the same number of d–d maxima in MeCN and $MeNO_2$ solution, the positions and intensities of these bands vary drastically, and in an unpredictable way, between these solvents. The UV spectra of **1**–**3a** in MeCN exhibit the same number of L^1Bu^t-based transitions, but with intensities that also vary markedly between the compounds. Since the Cl^- ligands in **2** and **3** do not de-coordinate in solution, this solvatochromism must reflect partial solvolysis of the L^1Bu^t ligand upon dissolution of **1**–**3a**. While ligand solvolysis is not significant in solutions of $[Cu(L^1R)_2]^{2+}$ (R = H, Mes),[1,3] intramolecular steric repulsion involving the bulky *tert*-butyl substituents may promote decoordination of L^1Bu^t in solution. In addition to d–d and L^1Bu^t-based bands, **2** and **3a** exhibit absorptions between 463–495 nm that can be ascribed to Cl ⟶ Cu LMCT absorptions.[10] This further supports the conclusion that the Cl^- ligands in these complexes remain coordinated in solution.

EPR spectroscopy and magnetochemical properties

X-Band EPR spectra of the Cu(II) compounds were run at 110 K, both as powders and in frozen 10 : 1 MeCN : toluene or $MeNO_2$: toluene solution (Table 3). The solution spectra of all three compounds are notably solvent-dependent, consistent with their UV/vis behaviour. In each solvent **1** and **3a** show similar, but not identical, axial $g_{||} > g_\perp > g_e$ EPR signals indicative of a $\{d_{x^2-y^2}\}^1$ or $\{d_{xy}\}^1$ Cu(II) ion (Fig. 4). This is consistent with these complexes forming tetragonal Cu(II) species in solution, although the more detailed nature of these solvolysed complexes is uncertain.[11] The solution EPR spectra of **2** are discussed below.

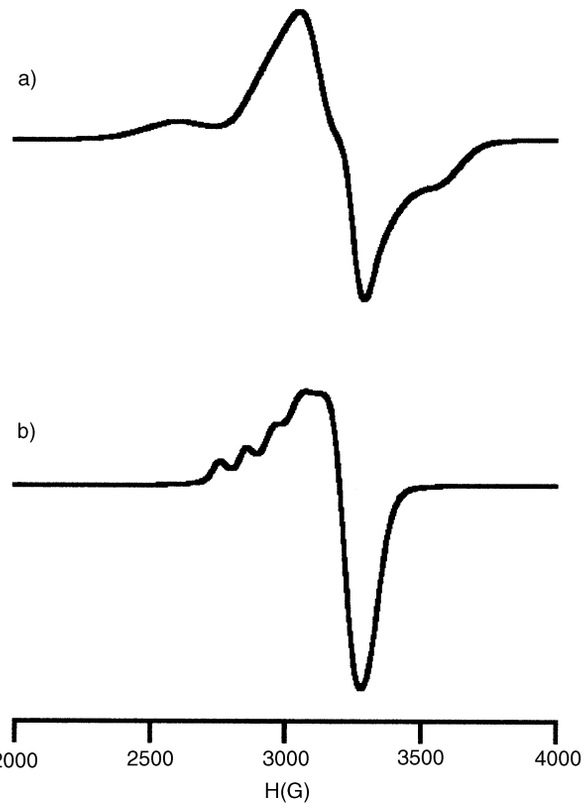

Fig. 4 X-Band EPR spectra of **3a** at 120 K (a) as a powdered solid; and (b) in 10 : 1 MeCN : toluene solution. The weak half-field resonance near 1500 G in the powder spectrum is not shown.

The EPR spectrum of solid **1** exhibits an 'inverse' $g_\perp > g_{||} \approx g_e$ pattern with no resolved hyperfine coupling that, in principle, implies a $\{d_{z^2}\}^1$ ground state for the complex.[11] This would indicate a trigonal bipyramidal stereochemistry at copper, which is clearly inconsistent with the crystal structure of **4** (see above). While it is possible that the conversion of **4** to **1** upon exposure to the atmosphere results in a large change in coordination geometry, this seems unlikely since the transformation does not cause a significant colour change. Alternatively, this may be a crystal spectrum rather than a molecular one, with anomalous *g*-values reflecting the relative orientations of adjacent $\{d_{x^2-y^2}\}^1$ or $\{d_{xy}\}^1$ spins in the solid.[12] In the absence of a crystal structure of **1**, it is impossible to distinguish between these possibilities.

The EPR spectrum of **2** is rhombic in the solid state and in solution, with a $g_1 > g_2 > g_3 > g_e$ pattern and no detectable $A\{^{63,65}Cu\}$ couplings. Although the *g*-values vary significantly between the spectra, their similar form in both phases suggests that they are true molecular spectra, and that **2** adopts qualitatively similar molecular structures in solution and the solid state. The powder spectrum was also run at Q-band, which yielded essentially identical *g*-values to the X-band spectrum. This confirms that **2** contains isolated $S = 1/2$ centres (*cf.* **3a**, see below). The *g*-values observed for **2** resemble those of $[CuX_2(terpy)]$ (X^- = Br^-, I^-, NCS^-, $NCSe^-$), which exhibit unusual C_{2v} geometries derived from a distorted trigonal bipyramid.[13,14] The d–d maxima exhibited by **2** in solution ($\lambda_{max} > 900$ nm) also occur at an abnormally long wavelength for a square-pyramidal complex,[15] but resemble those shown by $[CuI_2(terpy)]$.[13] Therefore, since **2** is a non-electrolyte in solution, it can be tentatively formulated as a molecular compound $[CuCl_2(L^1Bu^t)]$, with a sterically imposed C_{2v}-distorted structure.

The powder spectrum of **3a** is unusually complex (Fig. 4), and contains a weak half-field feature whose relative intensity is

Table 3 EPR data for the Cu(II) complexes in this study at 110 K. Hyperfine couplings are to ^{63,65}Cu. Parameters for powder spectra are derived from spectra run at Q-band, while solution spectra were obtained at X-band

		g_1	g_2	g_3	A_1/G	$\|D\|$/cm^{-1}	$\|E\|$/cm^{-1}
$[Cu(OH_2)_2(L^1Bu^t)][BF_4]_2$ (**1**)	Powder	2.232	2.232	2.005	—	—	—
	MeCN	2.347	2.082	2.082	128	—	—
	$MeNO_2$	2.296	2.071	2.071	150	—	—
$[CuCl_2(L^1Bu^t)]$ (**2**)	Powder	2.267	2.214	2.065	—	—	—
	MeCN	2.253	2.174	2.061	—	—	—
	$MeNO_2$	2.257	2.206	2.054	—	—	—
$[\{Cu(\mu\text{-}Cl)(L^1Bu^t)\}_2][BF_4]_2$ (**3a**)	Powder	2.306	2.073	2.065	—	0.035	0.009
	MeCN	2.301	2.097	2.097	100	—	—
	$MeNO_2$	2.251	2.076	2.076	155	—	—

greater at S-band compared to at X-band. This is diagnostic of an exchange-coupled system. The spectrum could be simulated on the basis of a zero-field-split $S = 1$ spin system, with the parameters listed in Table 3. This interpretation was confirmed by running this spectrum at S-band and at Q-band; these spectra were also well-reproduced using the parameters derived at X-band. The EPR parameters for **3a** resemble those derived from two other EPR studies of exchange-coupled $[Cu_2(\mu\text{-}Cl)_2]^{2+}$ complexes.[16,17] An alternative attempt to simulate these spectra using non-coincident axes for the g and D tensors was unsuccessful.

The observation of a spin-triplet EPR signal for solid **3a** must reflect weak superexchange between two adjacent Cu(II) centres which, presumably, is mediated *via* their weak association into dimers (Fig. 1). To quantify this, variable temperature susceptibility data were collected for a ground crystalline sample of **3a** between 330 and 5 K. Above 40 K, $\chi_M T$ is essentially constant at 0.84(1) cm^3 mol^{-1} K per dicopper unit, which agrees well with the spin-only value for two non-interacting $S = 1/2$ spins, of 0.76 cm^3 mol^{-1} K.[18] Below 40 K, $\chi_M T$ decreases, reaching 0.55 cm^3 mol^{-1} K at 5 K, which is consistent with weak antiferromagnetic coupling between the dicopper centres. A fit of the data was obtained using the Bleaney–Bowers equation for two Cu(II) ions,[18] with $g = 2.15(1)$ and $2J = -4.2(6)$ cm^{-1} for the $H = -2J(S_1S_2)$ Hamiltonian and a correlation coefficient of 0.990. No corrections for intermolecular interactions, paramagnetic impurities or temperature-independent paramagnetism were required for this analysis. The g-value refined by this method is in excellent agreement with the isotropic g-value obtained from the solid-state EPR spectrum.

Three different empirical magnetostructural correlations have been previously proposed for $[Cu_2(\mu\text{-}Cl)_2]^{2+}$ dimers of tetragonal Cu(II) ions linked by weak apical Cu ··· Cl interactions.[17,19,20] Given that superexchange in these compounds is almost always very weak ($|2J| \leqslant 15$ cm^{-1}), they are likely to be sensitive to the identity of the ligands present[21] and may be 'contaminated' by unresolved intermolecular interactions. Hence, it seems unlikely that a reliable magnetostructural correlation can be derived for these complexes by inspection of the available data. Nonetheless, we note that the value of $2J$ shown by **3a** agrees well with that exhibited by $[\{CuCl(\mu\text{-}Cl)(tmen)\}_2]$, which exhibits similar metric parameters to **3a** (Table 1) within its $[Cu_2(\mu\text{-}Cl)_2]^{2+}$ core [Cu–(μ-Cl) = 2.264(3) and 3.147(4) Å, Cu–(μ-Cl)–Cu = 96.8(1)°, $2J = -5.6$ cm^{-1}].[19,22]

Electrochemistry

Cyclic voltammograms (CVs) of **1** and **3a** were run in MeCN or acetone containing 0.1 M NBu_4BF_4 at 293 K. A similar study of **2** was not possible, owing to its poor solubility.

The CV of **1** in acetone exhibits a *quasi*reversible Cu(II/I) couple at $E_{1/2} = +0.15$ V ($\Delta E_p = 200$ mV, $I_{pa} : I_{pc} = 1.0$). An essentially identical CV is exhibited by the dimeric Cu(I) complex $[\{Cu(\mu\text{-}L^1Bu^t)\}_2][PF_6]_2$[23] under the same conditions. However, the CV of **1** in MeCN is rather different, showing an irreversible Cu(II/I) reduction at $E_{pc} = +0.21$ V, with a daughter Cu(II/I) reoxidation at $E_{pa} = +0.73$ V. In addition to these processes, **1** exhibits an irreversible Cu(I/0) reduction at $E_{pc} = -0.53$ V (acetone) or -0.89 V (MeCN), with an associated intense Cu desorption peak. The Cu(I/II) and Cu(I/0) couples in MeCN correspond closely to those exhibited by $[Cu(NCMe)_4]BF_4$,[24] which exhibits the same processes at $E_{pa} = +0.71$ and $E_{pc} = -0.85$ V under our conditions. We therefore conclude that reduction of **1** in MeCN results in rapid solvolysis of the resultant Cu(I) product, while reduction of **1** in acetone cleanly and reversibly affords $[\{Cu(\mu\text{-}L^1Bu^t)\}_2]^{2+}$.

The CV of **3a** in MeCN exhibits an irreversible Cu(II/I) and Cu(I/0) reductions at $E_{pc} = +0.08$ and -0.89 V, respectively. The first reduction exhibits two daughter processes assignable to Cu(I/II) reoxidations, at $E_{pa} = +0.38$ and $+0.70$ V, which both exhibit $I_{pa} : I_{pc} \cdot 0.4$ compared to the parent reduction. No peak that might be assigned to the oxidation of free Cl^- (E_p 1.0 V) was observed. From comparison with the CVs of **1** and $[Cu(NCMe)_4]BF_4$, it appears that reduction of **3a** to Cu(I) results in *partial* solvolysis of the complex over the voltammetric timescale, yielding $[Cu(NCMe)_4]^+$ and an unknown Cu(I) Cl^--containing species.

Concluding remarks

We have shown that the L^1Bu^t ligand is sufficiently bulky to cleanly form $[CuCl_x(solv)_{2-x}(L^1Bu^t)]^{(2-x)+}$ ($x = 2$, **2**; $x = 1$, solv = H_2O, **3**; $x = 2$, solv = H_2O, **1**; $x = 2$, solv = MeCN, **4**) complexes, but is too bulky to afford $[Cu(L^1Bu^t)_2]^{2+}$. In the solid state, **3a**, **3b** and **4** (and hence, presumably, **1**) adopt tetragonal stereochemistries. However, the spectroscopic properties of **2** are unusual and suggest that this complex may adopt a C_{2v}-distorted trigonal bipyramidal geometry.

The solution chemistry of **1**–**3a** is complex, and probably involves significant solvolysis of the L^1Bu^t ligand. This solution lability appears to be a general phenomenon for complexes of pyrazolylpyridine ligands bearing relatively bulky substituents,[25] and probably arises from a combination of steric repulsions involving the ligand substituents, and the relatively low basicity of the pyrazole N-donor atoms.[26] This may have a bearing on the fact that we are only aware of two reports of the use of L^1R complexes as catalysts.[27] In contrast, complexes of isosteric 4,4″-disubstituted-2,6-bis(4,5-dihydrooxazol-2-yl)pyridine (PyBox) ligands have been widely studied as asymmetric catalysts for alkene cyclopropanation, oxidation and polymerisation reactions, and aldol addition, among others.[28] The lability of coordinated L^1R ligands with bulky 'R' groups would afford heterogeneous catalytic sites in solution. This might easily lead to their complexes exhibiting poorer catalytic properties than for the more strongly coordinating PyBox ligand system.

Experimental

Unless stated otherwise, all manipulations were performed in air using commercial grade solvents. L^1Bu^t,[8] $[\{Cu(\mu\text{-}L^1Bu^t)\}_2]$-

$[PF_6]_2$[23] and $[Cu(NCMe)_4]BF_4$[24] were prepared by the literature procedures, while anhydrous $CuCl_2$ was prepared by heating $CuCl_2 \cdot 2H_2O$ (Avocado) at 100 °C for a week. $Cu(BF_4)_2 \cdot 6H_2O$ and $AgBF_4$ (Avocado) were used as supplied.

Synthesis of [2,6-bis(3-*tert*-butylpyrazol-1-yl)pyridine]-diaquacopper(II) ditetrafluoroborate (1)

Addition of L^1Bu^t (0.20 g, 6.4×10^{-4} mol) to a solution of $Cu(BF_4)_2 \cdot 6H_2O$ (0.22 g, 6.4×10^{-4} mol) in MeCN at room temperature gave a deep brown solution. This solution was concentrated to *ca.* 5 cm^3 and filtered. Vapour diffusion of Et_2O into this solution yielded lilac blocks, which rapidly lost crystallinity upon drying *in vacuo*. Yield 0.36 g, 90%. Found C, 37.8; H, 4.9; N, 11.9%. Calc. for $C_{19}H_{29}B_2CuF_8N_5O_2$ C, 38.2; H, 4.9; N, 11.9%. IR spectrum (nujol): 1610m, 1598s, 1535s, 1267s, 1060vs, 811s, 798m, 729m, 525s cm^{-1}. UV/vis (MeCN): λ_{max} = 210 nm (ε_{max} = 9,000 M^{-1} cm^{-1}), 244 (sh), 249 (22,400), 272 (24,000), 279 (26,800), 322 (16,500), 334 (sh), 507 (38), 748 (76). UV/vis ($MeNO_2$): λ_{max} = 541 nm (ε_{max} = 70 M^{-1} cm^{-1}), 746 (154). Conductivity (MeCN): Λ_M = 224 Ω^{-1} cm^2 mol^{-1}. Conductivity ($MeNO_2$): Λ_M = 137 Ω^{-1} cm^2 mol^{-1}. FAB mass spectrum (fragment): *m/z* 405 ($[^{63}CuF(L^1Bu^t)]^+$), 386 ($[^{63}CuF(L^1Bu^t)]^+$) with correct isotopic distributions.

Synthesis of dichloro[2,6-bis(3-*tert*-butylpyrazol-1-yl)pyridine]-copper(II) (2)

A suspension of L^1Bu^t (0.45 g, 1.4×10^{-3} mol) and $CuCl_2$ (0.18 g, 1.4×10^{-3} mol) in MeCN (75 cm^3) was stirred for 1 h at room temperature, until all the brown $CuCl_2$ had dissolved. The resultant yellow precipitate was filtered, and the pale yellow supernatant concentrated to *ca.* one-third its original volume, yielding a second crop of product. The two batches of solid were combined, washed with Et_2O and dried *in vacuo*. This product was analysed without further purification. Yield 0.51 g, 86%. Found C, 49.5; H, 5.5; N, 15.2%. Calc. for $C_{19}H_{25}Cl_2CuN_5$ C, 49.8; H, 5.5; N, 15.3%. IR spectrum (nujol): 1612s, 1599s, 1530s, 1316s, 1259s, 1177m, 1171m, 1060m, 998s, 966s, 938m, 791s, 771s, 676m cm^{-1}. UV/vis (MeCN): λ_{max} = 209 nm (sh), 245 (sh), 251 (ε_{max} = 46,100 M^{-1} cm^{-1}), 270 (17,400), 275 (sh), 311 (27,100), 335 (sh), 463 (763), 940 (83). UV/vis ($MeNO_2$): λ_{max} = 468 nm (ε_{max} = 391 M^{-1} cm^{-1}), 916(69). Conductivity (MeCN): Λ_M = 18 Ω^{-1} cm^2 mol^{-1}. Conductivity ($MeNO_2$): Λ_M = 11 Ω^{-1} cm^2 mol^{-1}. FAB mass spectrum (fragment): 421 ($[^{63}Cu^{35}Cl(L^1Bu^t)]^+$), 386 ($[^{63}Cu(L^1Bu^t)]^+$) with correct isotopic distributions.

Synthesis of dichlorobis[2,6-bis(3-*tert*-butylpyrazol-1-yl)-pyridine]dicopper(II) tetrafluoroborate (3)

To a suspension of **2** (0.25 g, 5.5×10^{-4} mol) in MeCN (25 cm^3) at room temperature was added $AgBF_4$ (0.11 g, 5.5×10^{-4} mol). The yellow starting material rapidly dissolved, yielding a brown solution and white AgCl precipitate. The solution was filtered and concentrated to *ca.* 3 cm^3. Vapour diffusion of Et_2O into this solution gave a mixture of green and amber cubic crystals, which were washed with Et_2O and dried *in vacuo*. Yield 0.27 g, 94%. The major green product analysed as $[\{Cu(\mu\text{-}Cl)(L^1Bu^t)\}_2][BF_4]_2$ (**3a**). Found C, 44.9; H, 4.9; N, 14.0%. Calc. for $C_{38}H_{50}B_2Cl_2Cu_2F_8N_{10}$ C, 44.8; H, 4.9; N, 13.8%. IR spectrum (nujol): 3488m, 1625s, 1594s, 1532m, 1318s, 1263s, 1217m, 1182m, 1060vs, 965m, 935m, 795s, 784s, 686m, 525m cm^{-1}. UV/vis (MeCN): λ_{max} = 209 nm (ε_{max} = 17,700 M^{-1} cm^{-1}), 227 (sh), 250 (20,900), 273 (23,500), 280 (23,200), 321 (15,800), 334 (sh), 483 (89), 805 (sh), 951 (104). UV/vis ($MeNO_2$): λ_{max} = 495 nm (ε_{max} = 117 M^{-1} cm^{-1}), 715 (77), 882 (81). Conductivity (MeCN): Λ_M = 124 Ω^1 cm^2 mol^{-1}. Conductivity ($MeNO_2$): Λ_M = 78 Ω^{-1} cm^2 mol^{-1}. FAB mass spectrum (fragment): 421 ($[^{63}Cu^{35}Cl(L^1Bu^t)]^+$), 386 ($[^{63}Cu(L^1Bu^t)]^+$) with correct isotopic distributions. The minor amber product analysed as $[\{Cu(\mu\text{-}Cl)(OH_2)(L^1Bu^t)\}_2][BF_4]_2$ (**3b**). Found C, 43.3; H, 5.1; N, 13.2%. Calc. for $C_{38}H_{54}B_2Cl_2Cu_2F_8N_{10}O_2$ C, 43.3; H, 5.2; N, 13.3%. FAB mass spectrum (fragment): 421 ($[^{63}Cu^{35}Cl(L^1Bu^t)]^+$), 386 ($[^{63}Cu(L^1Bu^t)]^+$) with correct isotopic distributions.

Single crystal X-ray structure determinations

Single crystals of X-ray quality of $[\{Cu(\mu\text{-}Cl)(L^1Bu^t)\}_2][BF_4]_2$ (**3a**), $[\{Cu(\mu\text{-}Cl)(OH_2)(L^1Bu^t)\}_2][BF_4]_2$ (**3b**) and $[Cu(NCMe)_2(L^1Bu^t)][BF_4]_2$ (**4**) were grown by diffusion of ether into solutions of the complexes in MeCN. Experimental details from the structure determinations are given in Table 4. All structures were solved by direct methods (SHELXS 86[29]) and refined by full matrix least-squares on F^2 (SHELXL 97[30]), with H atoms placed in calculated positions.

CCDC reference numbers 175839–175841.

See http://www.rsc.org/suppdata/dt/b1/b111210b/ for crystallographic data in CIF or other electronic format.

X-Ray structure determination of $[\{Cu(\mu\text{-}Cl)(L^1Bu^t)\}_2][BF_4]_2$ (3a). During refinement, one *tert*-butyl group was found to be disordered over two equally occupied orientations. All C–C and 1,3-C ··· C distances within the disordered group were restrained to 1.53(2) and 2.50(2) Å, respectively. The BF_4^- anion was also disordered over two orientations, which were modelled with a 0.50 : 0.50 occupancy ratio. All B–F and F ··· F distances were restrained to 1.39(2) and 2.27(2) Å, respectively. All H atoms were placed in calculated positions and all non-H atoms were refined anisotropically.

X-Ray structure determination of $[\{Cu(\mu\text{-}Cl)(OH_2)(L^1Bu^t)\}_2][BF_4]_2$ (3b). During refinement, the BF_4^- anion were found to be disordered over two orientations, which were modeled with a 0.75 : 0.25 occupancy ratio. All B–F and F ··· F distances within the disordered anion were restrained to 1.36(2) and 2.22(2) Å, respectively. The H atoms for the aqua ligand were located in the difference map and allowed to refine freely; all other H atoms were placed in calculated positions. All non-H atoms with occupancy >0.5 were refined anisotropically.

X-Ray structure determination of $[Cu(NCMe)_2(L^1Bu^t)][BF_4]_2$ (4). During refinement, one of the BF_4^- anions was found to be disordered over two sites, which were modelled with a 0.8 : 0.2 occupancy ratio. All B–F and F ··· F distances within this disordered anion were restrained to values of 1.36(2) and 2.22(2) Å, respectively. All non-H atoms with occupancy >0.5 were refined anisotropically, and all H atoms were placed in calculated positions.

Other measurements

Infrared spectra were obtained as Nujol mulls pressed between KBr windows between 400–4000 cm^{-1} using a Perkin–Elmer Paragon 1000 spectrophotometer. UV/visible spectra were obtained with a Perkin–Elmer Lambda 12 spectrophotometer, operating between 1100–200 nm, in 1 cm quartz cells. Positive ion fast atom bombardment mass spectra were performed on a Kratos MS890 spectrometer, employing a 3-NOBA matrix. CHN microanalyses were performed by the University of Cambridge Department of Chemistry microanalytical service. Conductivity measurements were obtained with a Jenway 4310 analyser, at concentrations of *ca.* 5×10^{-3} $mol.dm^{-3}$. All electrochemical measurements were carried out using an Autolab PGSTAT30 voltammetric analyser, in MeCN containing 0.1 M $NBu^n_4BF_4$ as supporting electrolyte. Cyclic voltammetric experiments employed platinum working and counter electrodes and a silver wire reference electrode; all potentials are referenced to an internal ferrocene/ferrocenium standard and were obtained at a scan rate of 100 mV s^{-1}.

Variable temperature magnetic susceptibility measurements were obtained using a Quantum Design SQUID magnetometer operating at 1000 G. A diamagnetic correction for the sample

Table 4 Experimental details for the single crystal structure determinations in this study

	[{Cu(μ-Cl)(L^{1}Bu^t)}$_2$][BF$_4$]$_2$ (**3a**)	[{Cu(μ-Cl)(OH$_2$)(L^{1}Bu^t)}$_2$][BF$_4$]$_2$ (**3b**)	[Cu(NCMe)$_2$(L^{1}Bu^t)][BF$_4$]$_2$ (**4**)
Formula	$C_{38}H_{50}B_2Cl_2Cu_2F_8N_{10}$	$C_{38}H_{54}B_2Cl_2Cu_2F_8N_{10}O_2$	$C_{23}H_{31}B_2CuF_8N_7$
M_r	1018.48	1054.51	642.71
Crystal system	Monoclinic	Monoclinic	Monoclinic
Space group	$P2_1/c$	$P2_1/c$	$P2_1/c$
a/Å	9.1630(1)	10.347(15)	9.794(3)
b/Å	12.9098(2)	11.521(7)	22.584(8)
c/Å	19.5616(3)	19.455(17)	13.690(5)
β/°	90.4727(6)	96.36(9)	110.09(2)
V/Å^3	2313.91(6)	2305(4)	2843.7(16)
Z	2	2	4
μ/mm^{-1}	1.107	1.117	0.848
T/K	100(2)	150(2)	150(2)
Measured reflections	41554	4291	6971
Independent reflections	5300	4054	5007
R_{int}	0.059	0.023	0.0424
$R(F)$[a], $wR(F^2)$[b]	0.037, 0.108	0.039, 0.104	0.057, 0.138
GOF	1.042	1.075	1.011

[a] $R = \Sigma[|F_o| - |F_c|]/\Sigma|F_o|$ [b] $wR = [\Sigma w(F_o^2 - F_c^2)/\Sigma wF_o^4]^{1/2}$

was estimated from Pascal's constants;[18] a diamagnetic correction for the sample holder was also applied. Observed and calculated data were refined using SIGMAPLOT.[31] EPR spectra were obtained using a Bruker ESP300E spectrometer: S-band spectra employed an ER4118SM-S-5W1 resonator and an ER4118VT cryostat; X-band spectra employed an ER4102ST resonator and ER4111VT cryostat; and Q-band spectra used an ER5106QT resonator and ER4118VT cryostat. Spectral simulations were performed using in-house software which has been described elsewhere.[32]

Acknowledgements

The authors thank Mr. J. Friend (University of Manchester) for the EPR spectra, and Dr. H. J. Blythe (University of Sheffield) for the magnetic susceptibility measurements. Funding by The Royal Society (M. A. H.), the EPSRC and ICI R&T Division (N. K. S.) and the University of Leeds is gratefully acknowledged.

References

1 N. K. Solanki, E. J. L. McInnes, F. E. Mabbs, S. Radojevic, M. McPartlin, N. Feeder, J. E. Davies and M. A. Halcrow, *Angew. Chem., Int. Ed.*, 1998, **37**, 2221.
2 A. J. Bridgeman, M. A. Halcrow, M. Jones, E. Krausz and N. K. Solanki, *Chem. Phys. Lett.*, 1999, **314**, 176.
3 N. K. Solanki, M. A. Leech, E. J. L. McInnes, J. P. Zhao, F. E. Mabbs, N. Feeder, J. A. K. Howard, J. E. Davies, J. M. Rawson and M. A. Halcrow, *J. Chem. Soc., Dalton Trans.*, 2001, 2083.
4 G. Wingefeld and R. Hoppe, *Z. Anorg. Allg. Chem.*, 1984, **516**, 223; K. Finnie, L. Dubicki, E. R. Krausz and M. J. Riley, *Inorg. Chem.*, 1990, **29**, 3908; M. Atanasov, M. A. Hitchman, R. Hoppe, K. S. Murray, B. Moubaraki, D. Reinen and H. Stratemeier, *Inorg. Chem.*, 1993, **32**, 3397; V. M. Masters, M. J. Riley and M. A. Hitchman, *J. Synchrotron Radiat.*, 1999, **6**, 242.
5 J. M. Holland, X. Liu, J. P. Zhao, F. E. Mabbs, C. A. Kilner, M. Thornton-Pett and M. A. Halcrow, *J. Chem. Soc., Dalton Trans.*, 2000, 3316.
6 M. A. Leech, N. K. Solanki, M. A. Halcrow, J. A. K. Howard and S. Dahahoui, *Chem. Commun.*, 1999, 2245.
7 N. K. Solanki, M. A. Leech, E. J. L. McInnes, F. E. Mabbs, J. A. K. Howard, C. A. Kilner, J. M. Rawson and M. A. Halcrow, *J. Chem. Soc., Dalton Trans.*, 2002, 1295.
8 D. L. Jameson and K. A. Goldsby, *J. Org. Chem.*, 1990, **55**, 4992.
9 W. J. Geary, *Coord. Chem. Rev.*, 1971, **7**, 81.
10 E. I. Solomon, K. W. Penfield and D. E. Wilcox, *Struct. Bonding (Berlin)*, 1983, **53**, 1.
11 B. A. Goodman and J. B. Raynor, *Adv. Inorg. Chem.*, 1970, **13**, 135.
12 F. E. Mabbs and D. Collison, *Electron Paramagnetic Resonance of d Transition Metal Compounds*, Elsevier, Amsterdam, 1992, p. 73.
13 M. I. Arriortua, J. L. Mesa, T. Rojo, T. Debaerdemaeker, D. Beltrán-Porter, H. Stratemeier and D. Reinen, *Inorg. Chem.*, 1988, **27**, 2976; T. Rojo, A. Garcia, J. L. Mesa, J. Via and M. I. Arriortua, *Inorg. Chim. Acta*, 1988, **149**, 159.
14 A. Kutoglu, R. Allmann, J.-V. Folgado, M. Atanasov and D. Reinen, *Z. Naturforsch., Teil B*, 1991, **46**, 1193.
15 A. B. P. Lever, *Inorganic Electronic Spectroscopy*, Elsevier, Amsterdam, 2nd edn., 1984, pp. 554–572.
16 W. E. Estes, J. R. Wasson, J. W. Hall and W. E. Hatfield, *Inorg. Chem.*, 1978, **17**, 3657.
17 M. Rodriguez, A. Llobet, M. Corbella, A. E. Martell and J. Reibenspies, *Inorg. Chem.*, 1999, **38**, 2328.
18 C. J. O'Connor, *Prog. Inorg. Chem.*, 1982, **29**, 203.
19 W. E. Marsh, K. C. Patel, W. E. Hatfield and D. J. Hodgson, *Inorg. Chem.*, 1983, **22**, 511.
20 T. Rojo, M. I. Arriortua, J. Ruiz, J. Darriet, G. Villeneuve and D. Beltran-Porter, *J. Chem. Soc., Dalton Trans.*, 1987, 285.
21 R. Lucas, S. Liu and L. K. Thompson, *Inorg. Chem.*, 1990, **29**, 85.
22 E. D. Estes, W. E. Estes, W. E. Hatfield and D. J. Hodgson, *Inorg. Chem.*, 1975, **14**, 106.
23 N. K. Solanki, A. E. H. Wheatley, S. Radojevic, M. McPartlin and M. A. Halcrow, *J. Chem. Soc., Dalton Trans.*, 1999, 521.
24 G. J. Kubas, *Inorg. Synth.*, 1990, **28**, 68.
25 R. J. Less, J. L. M. Wicks, N. P. Chatterton, M. J. Dewey, N. L. Cromhout, M. A. Halcrow and J. E. Davies, *J. Chem. Soc., Dalton Trans.*, 1996, 4055; J. Elguero, A. Fruchier, A. de la Hoz, F. A. Jalón, B. R. Manzano, A. Otero and F. Gómez-de la Torre, *Chem. Ber.*, 1996, **129**, 589.
26 J. Elguero, E. Gonzalez and R. Jacquier, *Bull. Soc. Chim. Fr.*, 1968, 5009.
27 W.-H. Fung, W.-C. Cheng, W.-Y. Yiu, C.-M. Che and T. C. W. Mak, *J. Chem. Soc., Chem. Commun.*, 1995, 2007; D. L. Christenson, C. J. Tokar and W. B. Tolman, *Organometallics*, 1995, **14**, 2148.
28 A. K. Ghosh, P. Mathivanan and J. Cappiello, *Tetrahedron Asymm.*, 1998, **9**, 1; H. Nishiyama, *Enantiomer*, 1999, **4**, 569; J. S. Johnson and D. E. Evans, *Acc. Chem. Res.*, 2000, **33**, 325.
29 G. M. Sheldrick, *Acta Crystallogr., Sect. A*, 1990, **46**, 467.
30 G. M. Sheldrick, SHELXL-97, Program for the refinement of crystal structures, University of Göttingen, Germany, 1997.
31 SIGMAPLOT, Program for Tabulating, Modelling and Displaying Data (v. 5.0), SPSS Inc., Chicago, IL, 1999.
32 F. E. Mabbs and D. Collison, *Electron Paramagnetic Resonance of d Transition Metal Compounds*, Elsevier, Amsterdam, 1992, ch. 7.